Rock Mechanics and Rock Engineering (2018) 51:2433–2438
https://doi.org/10.1007/s00603-018-1494-1

TECHNICAL NOTE

An Alternative Approach for Representing the Data Provided by the Acoustic Emission Technique

Dimos Triantis[1] · **Stavros K. Kourkoulis**[2]

Received: 11 January 2018 / Accepted: 23 April 2018 / Published online: 4 May 2018

Keywords Acoustic emissions · Inter-event times · Acoustic activity · Marble · Cement-mortar

1 Introduction

Accurate knowledge of the spatiotemporal evolution of damage within mechanically loaded structural elements is of great importance for a wide range of engineering fields. In this direction, the acoustic emission (AE) technique has been long ago recognized as an extremely valuable and flexible tool, which permits monitoring and even quantifying dynamic processes within loaded structural elements. In specific cases, the data provided by the AE technique allow gaining some insight into the deformation mechanisms (Ohtsu 2010; Aggelis et al. 2013), and also they provide timely warning signals concerning forthcoming failure (Miller et al. 2005; Kourkoulis et al. 2018a, b).

In laboratory experiments, with specimens prepared according to the respective international standards and submitted to monotonically increasing load until the final fracture, the AE technique allows recording of a number of AE hits ranging from several hundreds to several tenths or even hundreds of thousands, depending on the material, the exact size of the specimen and the loading mode. The AE hits rate (hits per second) and the energy release rate are some of the parameters that characterize the acoustic emission activity and can provide direct information concerning the time rate of generation of micro-cracks (Vidya et al. 2013; Moradian et al. 2016). Moreover, proper elaboration of data concerning the average frequency and the rise time per amplitude (or simply the rise time) of the acoustic signals permits proper classification of the internal damage processes according to whether they are due to tensile micro-cracking (Mode-I) or due to shear (and friction) phenomena (Mode-II) or even due to a combination of the above, i.e., mixed-mode phenomena (Ohno and Ohtsu 2010; Aggelis 2011).

Usually the data recorded by the AE sensors during any type of experiment are represented and analyzed with the aid of plots using a logarithmic scale for the hits rate and the energy release given that the relation between these quantities and the respective mechanical ones (like for example load or stress) is strongly non-linear, at least after a specific load (or stress) threshold.

The aim of this study is to introduce an alternative way for the representation of the data concerning the acoustic activity, in an attempt to enlighten what happens during the very last loading steps just before the fracture of the specimens. This alternative representation is based on a function of the inter-event times (denoted from here on as F function), which is plotted in terms of an "inverse" time arrow [sometimes denoted as "time-to-failure" (Li and Ma 2014)] using logarithmic scales. In fact, the term "time-to-failure" denotes the time parameter $(t_f - t)$, where t_f is the time instant of fracture. The pros and cons of this representation are here analyzed taking advantage of data from three-point bending tests with specimens made of either concrete or marble.

2 An Alternative Way to Represent the AE Data: The Function $F(\tau)$

Representation and elaboration of the acoustic activity (or in other words of the AE hits rate) is here achieved by introducing a time function $F(\tau)$, which reflects the average frequency of occurrence of AE hits, in a time window of N consecutive hits.

✉ Stavros K. Kourkoulis
stakkour@central.ntua.gr

[1] Electronic Devices & Materials Laboratory, University of West Attica, Athens, Greece

[2] Laboratory for Testing and Materials, Department of Mechanics, School of Applied Mathematical and Physical Sciences, National Technical University of Athens, 157 73 Athens, Greece

In order to derive the function $F(\tau)$, the inter-event time intervals

$$\Delta t_i = t_i - t_{i-1}, \quad i = 2, 3, \ldots \tag{1}$$

of a sufficient number of N consecutive hits are used. The role of the exact numerical value assigned to N will be discussed in Sect. 4 (Discussion and Conclusions). In Eq. (1) t_i stands for the time instant of occurrence of the ith AE hit, and t_{i-1} stands for the time instant of occurrence of the previous one. Then, the mean value, τ, of the N inter-event times Δt_i is determined for each group of N consecutive hits, denoted from here on as τ_i, as follows:

$$\tau_i = \frac{t_{N+i-1} - t_{i-1}}{N}, \quad i = 2, 3, \ldots \tag{2}$$

Especially for τ_1 the above formula is modified as follows:

$$\tau_1 = \frac{t_N - t_1}{N}. \tag{3}$$

The mean average frequency of occurrence, F, of the AE hits within a given time window between t_{i-N} and t_i is defined as the reciprocal of τ_i:

$$F(\tau_i) = \tau_i^{-1}, \quad i = 1, 2, \ldots \tag{4}$$

Each value $F(\tau_i)$ of the function F is paired with the average value $\bar{t}_i$ of the time instants of the occurrence of the respective N hits. Therefore:

$$\bar{t}_i = \frac{1}{N} \sum_{i}^{N+i-1} t_i, \quad i = 1, 2, \ldots \tag{5}$$

Subsequently, moving to the following $(i+1)$ AE hit, a new value of the function F is calculated, namely the $F(\tau_{i+1})$, that stands for the time window of the following N consecutive hits, from the moment t_{i+1-N} to the moment t_{i+1}, and so on.

To illustrate the potentialities and capabilities of the function $F(\tau)$, advantage will be taken of the data recorded by the acoustic sensors during some characteristic three-point bending tests. As a first step the data are represented and analyzed both according to the familiar way (i.e., time variation of the hits per second) and, also, according to the alternative representation (i.e., in terms of the function $F(\tau)$), for comparison reasons. As a second step, additional examples are considered using exclusively the alternative representation in terms of $F(\tau)$, in order to highlight some crucial aspects of the damage processes. In order to ensure comparability of the results, the function $F(\tau)$ was derived using the same number of consecutive hits ($N=15$) for all tests.

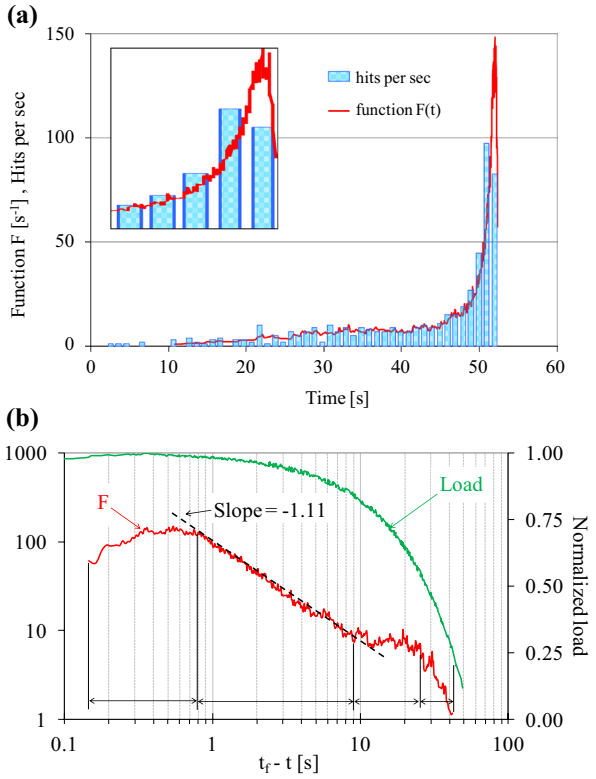

Fig. 1 **a** The time variation of the function F in juxtaposition to the respective evolution of the number of hits per sec, for a three-point bending test of a cement-mortar beam. The number of consecutive hits considered in order to determine the function F is $N=15$. In the embedded plot, a detailed view of the time evolution of both the function F and the number of hits per second during the last 5 s of the test is shown; **b** the function F plotted against the parameter $(t_f - t)$ using logarithmic scales, in juxtaposition to the respective load induced. It is seen that for the time interval with 8 s$<(t_f - t)<$9 s, a power law of the form $F=A(t_f - t)^{-m}$ perfectly describes the dependence of function F on $(t_f - t)$, with $m=1.11$

3 Some Characteristic Applications

The first application studied refers to the three-point bending of a prismatic cement-mortar beam of rectangular cross-section and overall dimensions $190\times45\times45$ mm^3. The sample was prepared using a cement-mortar mixture containing ordinary Portland cement, sand of fine aggregates and water in a ratio of 1:3:0.5, respectively (Stergiopoulos et al. 2015). The size of the fine aggregates was relatively small, ranging from approximately 0.6 mm to about 1.8 mm, thus resulting in a specimen of relatively low heterogeneity. The beam was loaded under load-control conditions at a constant rate equal to about 64 N/s. The load was applied monotonically up to the fracture of the specimen. A small preload of 0.2 kN was applied and the fracture load attained was $L_f = 3.37$ kN (Stavrakas et al. 2016). The duration of the test was equal to 52 s.

In Fig. 1a, the time variation of the acoustic activity is plotted according to both the traditional approach (hits per second) and also according to the function $F(\tau)$, which, in fact, corresponds to the mean occurrence of AE hits. As it could be expected, the time evolution of the function $F(\tau)$ follows closely the respective evolution of the hits per sec. Both plots appear to consist of three well distinguishable parts: For the major part of the loading procedure, i.e., for the time interval with 0 s < t < 46 s, both plots increase almost linearly with a very low slope. During the next 5 s, a dramatic amplification of the acoustic activity is observed, leading both plots to a global maximum just 1 s before the macroscopic fracture of the beam, as it can be seen more clearly in the graph embedded in Fig. 1a. Finally, during the last second, the acoustic activity starts decreasing. It is obvious, that this very last loading stage should be studied more thoroughly, since it corresponds to the peak of the processes that eventually lead to macroscopic failure and the respective data are very densely packed. It is thus quite possible that critical information remains hidden.

In this context, the time evolution of the function $F(\tau)$ is plotted in Fig. 1b versus the $(t_f - t)$ variable, i.e., according to an "inverse" time arrow, using logarithmic scales (which offer a "magnified" view of what happens during the very last loading stage), in juxtaposition to the respective evolution of the load induced. Regarding the early stages of the loading procedure, it is observed that, for the time interval with $(t_f - t) > 22$ s, the values of the function $F(\tau)$ increase (although with strong fluctuations), indicating the generation of new micro-cracks. Then, when 9 s$<(t_f - t)<$22 s, the function $F(\tau)$ is practically stabilized (with a certain degree of variability) corresponding perhaps to a stage of growth of the micro-cracks already generated during the previous time interval. In the next time interval, i.e., the interval with 0.8 s$<(t_f - t)<$9 s [which corresponds to a "load-interval" ranging from about 85% to almost 99% of the maximum load (L_f) attained (Stavrakas et al. 2016)] the function $F(\tau)$ starts increasing again. Within the specific time interval a power law of the form:

$$F = A\left(t_f - t\right)^{-m} \tag{6}$$

seems to perfectly describe the time variation of the function $F(\tau)$, with $m = 1.11$. This stage is probably related to an intense rate of growth of the existing micro-cracks and a potential initiation of their coalescence, which lead to the formation of macro-cracks. During the next time interval, i.e., for $(t_f - t) < 0.8$ s, it seems that the values of the function $F(\tau)$ are initially stabilized at a high level, exhibiting fluctuations typical of unstable crack growth. After the $(t_f - t) = 0.3$ s time instant the values of the function $F(\tau)$ start decreasing. This decrease is, probably, related to the fact that due to the formation and propagation of the fatal macro-crack (or macro-cracks) the strain energy available for the formation of new surfaces is consumed by the propagating front of this macro-crack and therefore there is no strain energy available to maintain a high rate of generation of new micro-cracks, resulting to decrease of the values of $F(\tau)$.

The second application considered refers again to a three-point bending test with a prismatic cement-mortar beam. The difference is that although the beam has almost the same overall dimensions as previously ($200 \times 50 \times 50$ mm^3), the size of the fine aggregates is bigger, ranging from 0.6 to 3.0 mm, resulting in an increased degree of heterogeneity. The load was again applied monotonically at a rate of 35 N/s until the fracture of the beam at L_f = 3.65 kN. The function $F(\tau)$ for the specific test is plotted in Fig. 2a against the $(t_f - t)$ parameter using logarithmic scales. The plot of Fig. 2a exhibits the same qualitative characteristics with those of Fig. 1b, and could be again divided in more or less the same well distinguishable time intervals. The main

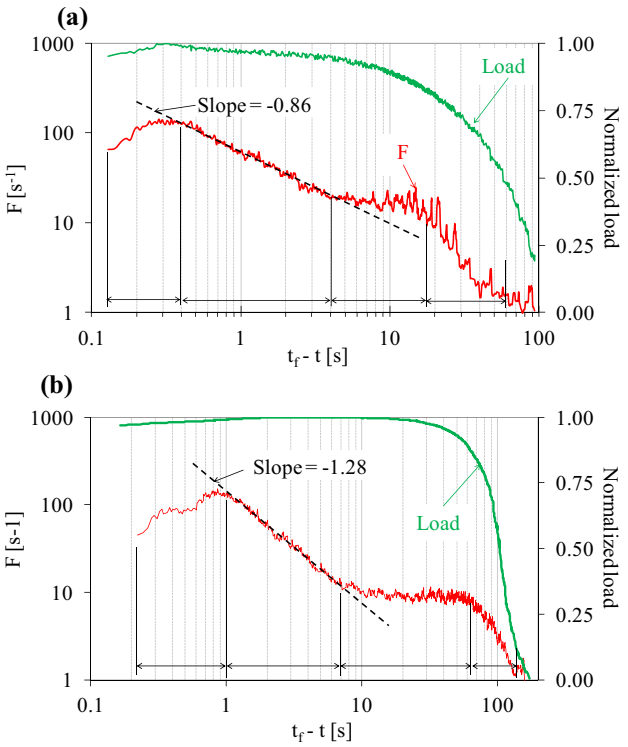

Fig. 2 **a** The function F plotted against the parameter $(t_f - t)$ using logarithmic scales, in juxtaposition to the respective load induced, for a three-point bending test of a cement-mortar beam with increased degree of heterogeneity. It is seen that for the time interval with 0.4 s$<(t_f - t)<$4 s, a power law of the form $F = A \cdot (t_f - t)^{-m}$ perfectly describes the dependence of function F on $(t_f - t)$, with $m = 0.86$; **b** The function F plotted against the parameter $(t_f - t)$ using logarithmic scales, in juxtaposition to the respective load induced, for a three-point bending test of a Dionysos marble beam of very fine internal structure. It is seen that for the time interval with 0. 1 s$<(t_f - t)<$7 s, a power law of the form $F = A(t_f - t)^{-m}$ perfectly describes the dependence of function F on $(t_f - t)$, with $m = 1.38$

difference is that the fluctuations observed during the first two time intervals (i.e., 4 s$<(t_f-t)<15$ s and $(t_f-t)>15$ s) are now much more intense, indicating the increased heterogeneity of the beam tested. Again, a power law of the same form with that of Eq. (6) perfectly describes the intermediate time interval (i.e., for 0.4 s$<(t_f-t)<4$ s), but now with $m=0.86$.

As a third application, a three-point bending test with a prismatic beam made of Dionysos marble is considered. The overall dimensions of the marble beam were $20\times20\times100$ mm^3. Dionysos marble is characterized by very fine internal structure resulting to a very low degree of heterogeneity, independently of the size of the specimen. The test was now implemented under displacement-control conditions at a constant displacement rate equal to 0.17 mm/s. The function $F(\tau)$ for the specific test is plotted in Fig. 2b, again versus the (t_f-t) parameter using logarithmic scales. The qualitative characteristics of the plot are quite similar to those of the previous two tests; however, the fluctuations of the time variation of the function $F(\tau)$ are much smoother and of much lower amplitude, reflecting the extremely fine internal structure of the specific variety of marble (Kourkoulis et al. 1999). Again the intermediate portion of the plot (i.e., that with 1 s$<(t_f-t)<7$ s) is very well described by the power law of Eq. (6), with $m=1.28$.

4 Discussion and Concluding Remarks

An alternative approach for representing and analyzing the data collected by the acoustic sensors, during mechanical loading of specimens made of brittle materials, like cement-mortar beams and marble, was introduced, in terms of the so-denoted $F(\tau)$ function, which reflects the average frequency of occurrence of AE hits, in a "sliding time window" of N consecutive hits. Concerning the numerical value of N, it is to be accepted that it is more or less an "arbitrary" choice. Indeed, it is not easy (or even permissible) to assign a specific numerical value to N. The choice depends on the specific test and the overall number of hits recorded during the whole duration of the test. The greater the overall number of hits recorded, the higher the value of N that can be adopted without shadowing critical details of the analysis. In fact, the value of N somehow describes the "resolution" of the analysis. Fortunately, the exact numerical value assigned to N does not significantly influence the results of the analysis, assuming of course that N is a relatively small fraction of the total number of hits recorded during the test's duration. In order to support the above point of view, the analysis for the first experiment discussed in the manuscript is here repeated, assigning to N two additional values, i.e., $N=10$ and $N=20$ (recall that the analysis described in Sect. 3 was implemented using a value equal to $N=15$). The results are plotted in Fig. 3. As it can be seen from this figure, all three plots are extremely close to each other and the overall conclusions drawn are not influenced at all. However, it is evident that decreasing the value of N results to slightly stronger local fluctuations while increasing the value of N results to smoother curves. Clearly, further research on the specific issue is required, in order to conclude whether an optimum number exists for the value of N and what this optimum value is.

The analysis of the experimental data in terms of the function $F(\tau)$ revealed that the acoustic activity at the critical time interval just before fracture of the specimen (excluding the very last second or seconds) obeys a power law. The scaling described in Eq. (6) as $F=A(t_f-t)^{-m}$ is in agreement with the so-called accelerated deformation law, observed in seismology before main events (see for example De Santis et al. 2015, Guilhem et al 2013, Papazachos et al. 2014, Tzanis and Vallianatos 2003), where in an observed physical parameter $\Omega(t)$ a scaling with $(t_f-t)^{-m}$ appears. The latter has been also observed in a number of rock fracture experiments, where acoustic emissions or pressure-stimulated currents (Davidsen et al. 2017; Vallianatos and Triantis 2008) were monitored and recorded. In the laboratory scale, experiments under uniaxial stress have shown that, a generalized expression of the well-known seismology Omori–Utsu law describes the rate of acoustic events before the failure point (Baró et al. 2013). Although similar conclusions concerning the evolution of acoustic activity in wood specimens (indicating, however, an exponential rather a power law), were also reported by Brunner et al. (2006), it is obvious that additional research is required to ensure that the specific law describes larger classes of materials and specimens of a wider range of dimensions under different loading schemes.

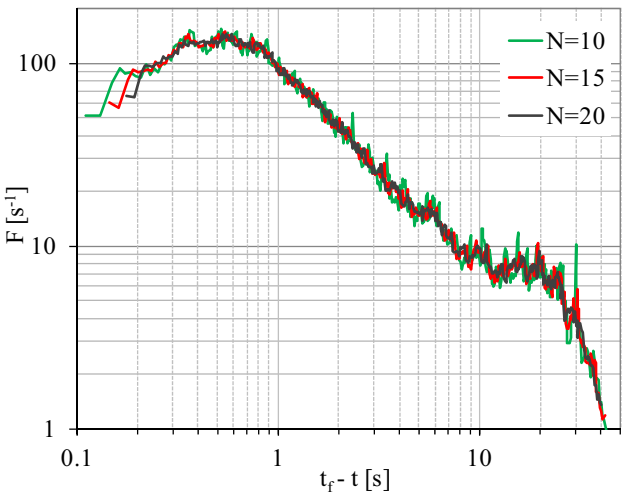

Fig. 3 The role of the numerical value assigned to N

Despite of any limitations, the as above-defined function $F(\tau)$ allows for a more informative representation of the acoustic activity within a given time period. Indeed, according to the traditional representation of the acoustic activity in terms of hits per second, the step is, by default, 1 s, or in other words there is only one piece of information for each step/second. On the other hand, adopting the $F(\tau)$ function the step is in fact the hit itself in combination with the number of consecutive N hits considered. In this way, more information is provided for each second. This is achieved because the alternative representation is based on the concept of a "sliding time window", the duration of which is variable depending on the inter-event times between successive hits. (In the first step of the analysis the N first hits, i.e., the hits from $n=1$ to $n=N$ are taken into consideration, in the second step the hits from $n=2$ to $n=N+2$ are considered, in the third step the hits from $n=3$ to $n=N+3$, etc.)

To make the above point clear, the two representations [the traditional one and that in terms of the function $F(\tau)$] are plotted in Fig. 4a in juxtaposition to each other, for the same set of data (i.e., those of the first experiment discussed in the manuscript), using for both plots logarithmic scales for the sake of a fair comparison. It is clear from Fig. 4a that the alternative representation based on the function $F(\tau)$ offers much more information, thus providing a deeper insight or, equivalently, a much "thinner" resolution of the time evolution of the acoustic activity.

The above-mentioned deeper insight is, obviously, assisted, by the fact that the function $F(\tau)$ is plotted versus the (t_f-t) variable (the "time-to-failure") on a log time scale, illustrating much more clearly the time evolution of the acoustic activity during the very last seconds (or even tenths of seconds) prior to the failure of the mechanically loaded specimens. It could be argued, perhaps, at this point that using logarithmic rather than natural scales for plotting the acoustic activity could result to distorted view of the trends of the quantities considered. This is, unfortunately, the penalty that has to be paid in case one wants to enlighten events at a specific narrow time interval (in the case studied here at the very last loading steps); however, in the applications considered in the present study this distortion does not hide critical details of the time evolution of the quantities considered. To make this point evident the same set of data used to plot Fig. 4a are plotted in Fig. 4b using natural scales. Considering Fig. 4a and Fig. 4b comparatively, it can be seen that the overall time evolution of both the function $F(\tau)$ and of the hits per second (in terms of the "inverse" time arrow, i.e., versus the (t_f-t) parameter) exhibits the same qualitative trends: They increase almost for the whole duration of the test (although at different rates during various time intervals) and only during the last second their values start decreasing. This behavior is common for both the natural and the logarithmic representation; however, the latter

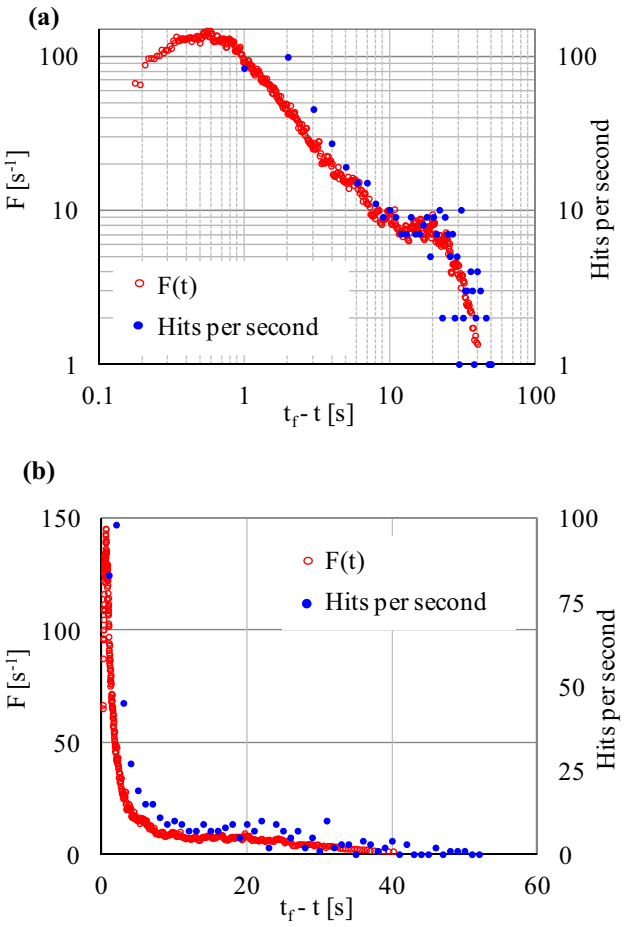

Fig. 4 The traditional representation of AE data and the respective one using the F function in: **a** logarithmic and **b** natural scales

provides a definitely more detailed view into the very last loading stages, balancing, thus, the loss of "common feeling" for the time evolution which is, obviously, closer to the plots in terms of natural rather logarithmic scales.

Before concluding, it should be mentioned that the correlation of the four distinct phases exhibited by the $F(\tau)-(t_f-t)$ plot is, as yet, somehow speculative. Indeed, the specific project (the data of which were discussed here) is still in full progress providing additional data supporting the conclusions presented in previous sections. This is seen in Fig. 5, in which the function $F(\tau)$ for a marble specimen under uniaxial compression is plotted, again versus the (t_f-t) parameter, in logarithmic scales. It is, at least, very encouraging to note that the qualitative characteristics of this plot are in excellent agreement with the respective ones already discussed (gathered from three-point bending tests). Moreover, the slope of the plot in the respective third time interval is again described according to an excellent manner by Eq. (6) with an m-value equal to $m=1.20$, very close to the value of $m=1.28$ derived for the marble specimen under

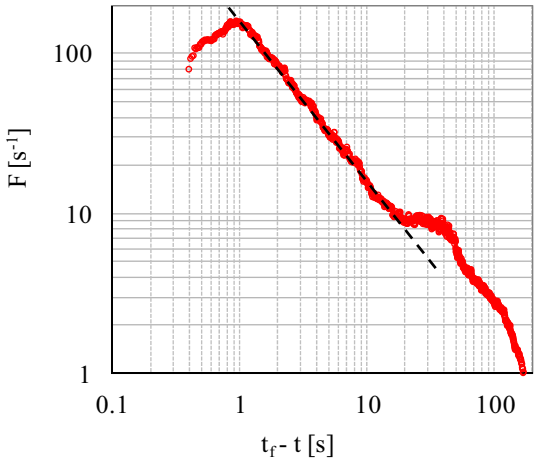

Fig. 5 Evolution of the *F* function for a uniaxial compression test of a prismatic marble specimen. The slope of the "linear" portion is now equal to − 1.20

three-point bending. In any case, additional characteristics of the acoustic events (like, for example, the energy and the duration of the acoustic events) must be taken into account, in order for a correlation between the acoustic activity and the internal damage processes (like, for example, generation of micro-cracks, crack propagation, coalescence of cracks, etc.) to be established. Obviously, for this goal to be achieved data from different experiments and a much wider range of materials must be considered.

Acknowledgements The authors express their sincere thanks to the two anonymous reviewers of the present manuscript. Their comments and suggestions were extremely valuable in the direction of significantly improving its quality and scientific integrity.

References

Aggelis DG (2011) Classification of cracking mode in concrete by acoustic emission parameters. Mech Res Com 38:153–157

Aggelis DG, Mpalaskas A, Matikas TE (2013) Acoustic signature of different fracture modes in marble and cementitious materials under flexural load. Mech Res Commun 47:39–43

Baró J, Corral Á, Illa X, Planes A, Saljes EKH, Schranz W, Soto-Parra DE, Vive E (2013) Statistical similarity between the compression of a porous material and earthquakes. Phys Rev Lett 110(8):088702

Brunner AJ, Howald MT, Niemz P (2006) Acoustic emission rate behaviour of laminated wood specimens under tensile loading. J Acoust Emiss 24:104–110

Davidsen J, Kwiatek G, Charalampidou E-M, Goebel T, Stanchits S, Rück M, Dresen G (2017) Triggering processes in rock fracture. Phys Rev Lett 119(6):068501

De Santis A, Cianchini G, Di Giovambattista R (2015) Accelerating moment release revisited: Examples of application to Italian seismic sequences. Tectonophysics 639:82–98

Guilhem A, Bürgmann R, Freed AM, Ali Tabrez S (2013) Testing the accelerating moment release (AMR) hypothesis in areas of high stress. Geophys J Int 195(2):785–798

Kourkoulis SK, Exadaktylos GE, Vardoulakis I (1999) U-notched Dionysos-Pentelicon marble in three point bending: The effect of nonlinearity, anisotropy and microstructure. Int J Fract 98(3–4):369–392

Kourkoulis SK, Pasiou ED, Dakanali I, Stavrakas I, Triantis D (2018a) Notched marble plates under tension: Detecting pre-failure indicators and predicting entrance to the "critical stage". Fatigue Fract Eng Mater Struct 41(4):776–786

Kourkoulis SK, Pasiou ED, Dakanali I, Stavrakas I, Triantis D (2018b) Notched marble plates under direct tension: Mechanical response and fracture. Constr Build Mater 167:426–439

Li XL, Ma SL (2014) Laboratory acoustic emission study for earthquake generation process. Earthq Sci 27(6):627–646

Miller RK, Hill EVK, Moore PO (2005) Nondestructive Testing Handbook, vol 6, Acoustic Emission Testing, 3rd edn. Chaps. 8 and 11, American Society for Nondestructive Testing ASNT, Columbus

Moradian Z, Einstein HH, Ballivy G (2016) Detection of cracking levels in brittle rocks by parametric analysis of the acoustic emission signals. Rock Mech Rock Eng 49:785–800

Ohno K, Ohtsu M (2010) Crack classification in concrete based on acoustic emission. Constr Build Mater 24:2339–2346

Ohtsu M (2010) RILEM TC 212-ACD: Acoustic emission and related NDE techniques for crack detection and damage evaluation in concrete. Mater Struct 43:1187–1189

Papazachos BC, Karakaisis G, Scordilis EM (2014) Time dependent seismicity in the continental fracture system. Bollettino di Geofisica Teorica ed Applicata 55(3):617–639

Stavrakas I, Triantis D, Kourkoulis SK, Pasiou ED, Dakanali I (2016) Acoustic emission analysis when cement mortar specimens are subjected to three point bending repetitive cycles. Lat Am J Solids Struct 13(12):2283–2297

Stergiopoulos C, Stavrakas I, Triantis D, Vallianatos F, Stonham J (2015) Predicting fracture of mortar beams under three-point bending using non-extensive statistical modelling of electric emissions. Phys A 419:603–611

Tzanis A, Vallianatos F (2003) Distributed power-law seismicity changes and crustal deformation in the EW Hellenic Arc. Nat Hazards Earth Syst Sci 3:179–195

Vallianatos F, Triantis D (2008) Scaling in pressure stimulated currents related with rock fracture. Phys A 387:4940–4946

Vidya SR, Prasad RV, Raghu Prasad BK, Rao MVMS. (2013) Microcracking and Fracture process in cement mortar and concrete: a comparative study using acoustic emission technique. Exp Mech 53:1161–1175